Lifetime of Strongly Correlated States on

**Near-Term Quantum Computers** 

Lillian I. Payne Torres, Anna O. Schouten, and David A. Mazziotti\*

Department of Chemistry and The James Franck Institute, The University of Chicago,

Chicago, IL 60637 USA

E-mail: damazz@uchicago.edu

Abstract

Here we study the lifetime of strongly correlated stationary states on quantum

computers. We find that these states develop a non-trivial time dependence due to the

presence of noise on current devices. After an exciton-condensate state is prepared,

its behavior is observed with respect to unitary operations that should preserve the

stationarity of the state. Instead of stationarity, however, we observe non-trivial time

dependence in which the large eigenvalue of the particle-hole reduced density matrix—

the exciton population of the condensate—decays towards unity, reflecting the loss

of entanglement and off-diagonal long-range order. The result offers insight into the

challenge of simulating strongly correlated systems on near-term quantum devices and

highlights the importance of developing novel strategies for error mitigation that can

preserve many-body correlations.

Introduction

Efficient and accurate modeling of strongly correlated quantum systems continues to be

a pressing challenge in the field of electronic structure theory, as strong correlation is re-

1

sponsible for many novel chemical phenomena such as atypical superconductors, topological insulators, and spin liquids. <sup>1–5</sup> However, the simulation of strongly correlated quantum systems on classical computers has often been stymied by the computational expense of such calculations. The unique features of quantum computers, namely coherence and entanglement, mean that the application of quantum computing to electronic structure theory has the potential to demonstrate significant advantage over classical computing in modeling correlated chemical systems. <sup>6–12</sup> Ideally, implementing electronic structure theory on quantum computers can provide significant speedup over classical computers, and even allow for solution of classically intractable problems. <sup>7–10</sup> While several algorithms have been developed to predict the electronic structure of chemical systems, <sup>9,11,13–22</sup> these methods are limited by the errors inherent to near-term intermediate-scale quantum (NISQ) computers. <sup>23–25</sup> In particular, the environmental noise experienced by near-term quantum computers leads to a breakdown of the system-wide entanglement and long-range order necessary for the quantum simulation of many-electron quantum systems. <sup>26,27</sup>

Currently, despite significant advances in understanding, mitigating, and correcting quantum device noise; <sup>28–39</sup> the limitations caused by device noise in the preparation of strongly correlated states are not well defined. In this work we directly probe the extent to which system-wide entanglement and long-range order can endure in a strongly correlated state prepared on a NISQ-era quantum device. We prepare a strongly correlated exciton condensate state on a quantum computer and observe its behavior with respect to unitary operations that should preserve the stationarity of the state. We observe instead non-trivial time dependence evidenced by the transition from the strongly-correlated condensate state originally prepared to an uncorrelated ensemble state. The breakdown of entanglement and long-range order is directly observable via the large eigenvalue of the particle-hole reduced density matrix— the exciton population of the condensate—which decays towards unity. We find that the lifetime and decay pattern of the strong correlation is dependent on the unitary operations used for propagation of the system, as well as the number of qubits used to pre-

pare the state. These investigations elucidate the challenges in simulating strongly correlated systems on near-term quantum devices as both stationary and time-dependent simulations will be impacted by the fictitious time evolution induced by noise. Our results underscore the importance of designing error mitigation techniques tailored to preserve system-wide entanglement and long-range order for the reliable simulation of strongly correlated systems.

# Theory

We use the signature of condensation of particle-hole pairs as the measure of correlation while the behavior of our chosen state, an exciton condensate state, is observed with respect to unitary operations in the presence of noise. Here we first detail our chosen strongly correlated state and describe the process of stationary-state evolution with noise. We then introduce our signature of exciton (or qubit) condensation, used as the measure of correlation in this study. Finally, we describe the use of orbital occupation numbers as a visualization of the state evolution in the presence of noise.

## **Correlated State Preparation**

While there are a diverse range of strongly correlated systems, our targeted investigation of the effects of noise on strong correlation and system-wide entanglement necessitates a simple strongly correlated state to serve as model of the quantum entanglement that is desirable for the modeling of strongly correlated systems. Several varieties of strongly correlated states have been prepared via superconducting qubits, including Cooper-pair and exciton condensate-like states. <sup>26,40–42</sup> Interpreting a qubit as a site consisting of one fermion in two orbitals, an exciton condensate-like state is a highly entangled state composed of particle-hole pairs condensed into a single quantum state. <sup>26</sup> The Greenberger-Horne-Zeilinger (GHZ) state exhibits maximal exciton condensate character for any number of qubits, corresponding to the maximal entanglement of particle-hole pairs. <sup>26</sup> The GHZ state for an N-qubit system

is described by:

$$|\Psi_{GHZ}\rangle = \frac{1}{\sqrt{2}}(|0\rangle^{\otimes N} + |1\rangle^{\otimes N}) \tag{1}$$

which is an ideal model system for the observation of noise effects on strong correlation and entanglement because it is a correlated state corresponding to the maximal entanglement of particle-hole pairs.

#### Time Evolution

If a highly correlated GHZ state is prepared and then subjected to a series of unitary operations that should preserve the stationarity of the state, all time-dependent behavior is the result of device noise. <sup>28</sup> We thus subject our prepared GHZ states to repeated unitary operations of the form  $\exp(-i\,\hat{O}\tau)$ , where  $\hat{O}$  is a scaled dimensionless operator. We can view each operation as applying a perturbation due to the device noise. As the operations themselves should not alter the prepared state, the perturbation and any time evolution resulting are solely the result of noise. We thus prepare exciton condensate GHZ states on a quantum device and evolve them according to  $\exp(-i\,\hat{O}(\omega)\tau)$ . A three-qubit operator:

$$\hat{O}_a = \omega \sigma_z^0 \otimes \sigma_z^1 + \omega \sigma_z^1 \otimes \sigma_z^2 + \omega \sigma_z^2 \otimes \sigma_z^0 \tag{2}$$

is used for preliminary investigations, where  $\sigma_z^j$  refers to the Pauli-Z matrix acting on the jth qubit and  $\sigma_z^j \otimes \sigma_z^i$  is a two-qubit tensor product. As  $R_{ZZ}(\theta) = \exp(-i\frac{\theta}{2}\sigma_z \otimes \sigma_z)$ , the unitary operations correspond to a series of  $R_{ZZ}$  gates. These  $R_{ZZ}$  gates can then be implemented as an  $R_Z$  rotation between two CNOT gates. The time t in each evolution is denoted as the number of  $R_{ZZ}$  operations multiplied by the dimensionless time step  $\tau$ , where  $\tau = \frac{1}{3}$ . To compare the relative effects of operators composed of single-qubit and two-qubit gates, we also calculate the unitary evolution of the GHZ state for a three-qubit perturbation operator

composed of unentangled single-qubit Pauli-Z operations:

$$\hat{O}_b = \omega \sigma_z^0 + \omega \sigma_z^1 + \omega \sigma_z^2 \tag{3}$$

A schematic demonstrating the quantum state preparations for the initial states and the first time evolution steps of  $\hat{O}_a$  and  $\hat{O}_b$  can also be found in the Supporting Information.

#### Signature of Qubit Condensation

In order to determine the presence and extent of strong correlation throughout our time evolution, a characteristic and calculable signature is required. Ideal for this purpose is the quantum signature of exciton (qubit) condensation from reduced density matrix (RDM) theory, i.e., an eigenvalue greater than one in the particle-hole reduced density matrix. <sup>43,44</sup> The particle-hole RDM has elements given by:

$${}^{2}G_{k,l}^{i,j} = \langle \Psi | \hat{a}_{i}^{\dagger} \hat{a}_{j} \hat{a}_{l}^{\dagger} \hat{a}_{k} | \Psi \rangle \tag{4}$$

where  $|\Psi\rangle$  is the N-electron wavefunction and  $\hat{a}_i^{\dagger}$  and  $\hat{a}_i$  are the fermionic creation and annihilation operators. <sup>43–45</sup> Additionally, one must subtract from the particle-hole RDM the component corresponding to a ground-state-to-ground-state transition, which otherwise creates one extraneous large eigenvalue unrelated to exciton condensation

$${}^{2}\tilde{G}_{k,l}^{i,j} = {}^{2}G_{k,l}^{i,j} - {}^{1}D_{j}^{i1}D_{k}^{l}. \tag{5}$$

An eigenvalue greater than one from this modified particle-hole RDM is the signature of exciton condensation. In the following sections we refer to the maximum eigenvalue of this matrix as  $\lambda_G$ . The eigenvalues of the modified particle-hole RDM correspond to the occupation of each particle-hole state. Garrod and Rosina<sup>44</sup> have shown that the eigenvalues of  ${}^2\tilde{G}$  are zero or one in the noninteracting limit and bounded above by  $\frac{N}{2}$  in the limit of

strong correlation.

#### Generalized Pauli Constraints

Orbital occupation numbers—the eigenvalues of the one-fermion RDM—provide a useful coordinate representation for the visualization of the condensate state. The eigenvalues of the one-fermion RDM are constrained, not only by the traditional Pauli constraints from the Pauli exclusion principle  $(0 \le n_i \le 1)$ , <sup>46</sup> but also by a set of further constraints arising from the requirement that the wavefunction be anti-symmetric. <sup>47,48</sup> For a three-qubit quantum system (a pure system of three electrons in six orbitals), <sup>49</sup> the relevant generalized Pauli constraints are

$$n_5 + n_6 - n_4 \ge 0, (6)$$

where

$$n_1 + n_6 = 1, (7)$$

$$n_2 + n_5 = 1, (8)$$

$$n_3 + n_4 = 1. (9)$$

Here each  $n_i$  corresponds to the natural-orbital occupations ordered from largest to smallest. <sup>50–54</sup> The smallest three orbital occupation numbers,  $n_4$ ,  $n_5$ , and  $n_6$ , can be plotted against two polytopes representing the imposed constraints: the so-called Pauli polytope containing the set of all possible occupations according to the Pauli constraints ( $0 \le n_i \le 1$ ) and the generalized Pauli polytope containing the set of all possible occupations according to the generalized Pauli constraint.

# Results

The noisy time evolution of the GHZ state is performed for an arbitrary value of  $\omega = 0.2$ . The orbital occupation numbers are calculated for each timestep of the evolution on a real quantum device (ibm\_kyoto) and on a noiseless quantum simulator.<sup>55,56</sup> These results are plotted in Figure 1. Here the Pauli polytope is the combination of yellow and blue regions allowed by  $0 \le n_i \le 1$ , while the generalized Pauli polytope is the yellow region allowed by Eq. 5. The  $(n_4, n_5, n_6) = (0.5, 0.5, 0.5)$  corner of the polytope corresponds to the occupation of the ideal GHZ state, and hence, points deviating from that corner represent a transition to a new quantum state.

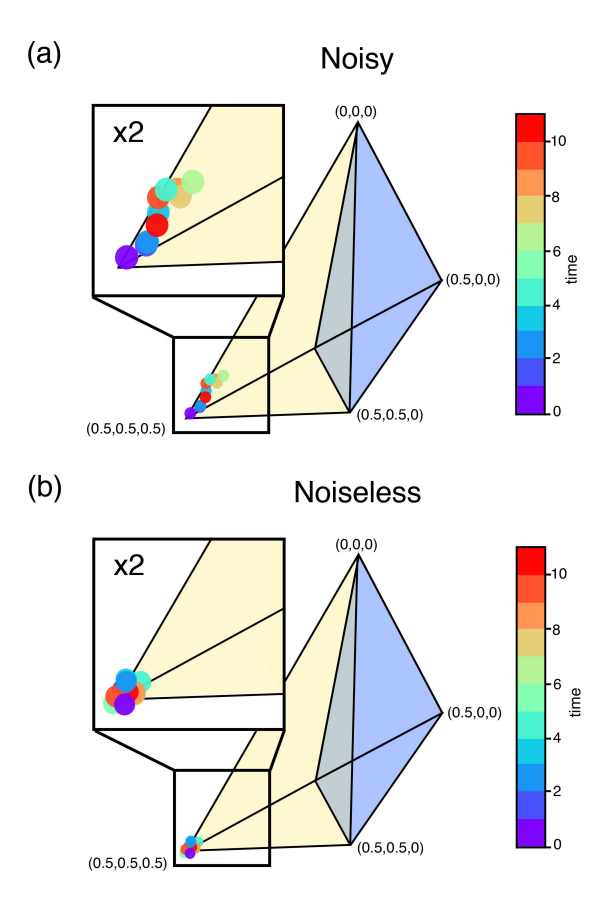


Figure 1: Experimental occupation numbers  $(n_4, n_5, n_6)$  from the propagation of  $\hat{O}_a$  on a noisy quantum device (a) and a noiseless quantum simulator (b). The color variation of the points (from violet to red) indicates the timestep. Occupation of the GHZ state is indicated by occupation of the vertex (0.5, 0.5, 0.5).

The orbital occupations from the noise-free simulator evolution show the system satu-

rating the (0.5, 0.5, 0.5) vertex for all timesteps, indicating unchanging occupation of the strongly correlated GHZ state. This confirms that, as intended, our unitary operations preserve the stationarity of the state in the absence of noise. However, the results for the real quantum device demonstrate that the occupations recede from the (0.5, 0.5, 0.5) vertex as the simulation progresses, indicating that the noise on the device is acting as a "fictitious force" that causes time evolution in a system that should remain stationary. Instead of remaining in the GHZ state, the system undergoes a transition to some new state characterized by orbital occupations in a new region of the polytope.

To understand the implications of the state transition observed via orbital occupation numbers on long-range order and system-wide entanglement, we examine the signature of qubit condensation mentioned previously. We compare the relative effects of operators composed of single-qubit and two-qubit gates by calculating the time evolution of the GHZ state for  $\hat{O}_a$  and  $\hat{O}_b$  with an arbitrary value of  $\omega = 0.2$ . The time evolution of  $\lambda_G$  for each operator is plotted in Figure 2, for both the actual quantum device (ibm\_kyoto), a noisy simulator generated from system snapshots, 55,57 and the noiseless quantum simulator. For the real quantum device, time evolution of  $\hat{O}_a$  yields a  $\lambda_G$  that decays for each time evolution step. Beginning at a value of  $\lambda_G = 1.46$ , after 10 time evolution steps  $\lambda_G$  decays to a value of approximately 0.88. The large eigenvalue at t=0 falls slightly below the ideal value of 1.5 due to errors occurring in the initial state preparation. As the three-qubit GHZ state requires 2 CNOT gates to prepare it, some noise during initial state preparation is unavoidable. 26 Calculating state fidelity allows us to ensure that we are approximating the desired GHZ state despite this deviation from ideal  $\lambda_G$ ; at t=0, we calculate a state fidelity of 0.953, showing that our prepared state is very close to the ideal GHZ state. As  $\lambda_G$  at t=0falls only 0.04 below the ideal value, this high state fidelity is unsurprising. The closeness of  $\lambda_G$  at t=0 to the ideal value of 1.5 clearly demonstrates off-diagonal long-range order and system-wide entanglement. However, this qubit condensate character decays such that  $\lambda_G$  falls below the threshold value of 1 by t=10, indicating the loss of entanglement and long-range order in ten time steps.

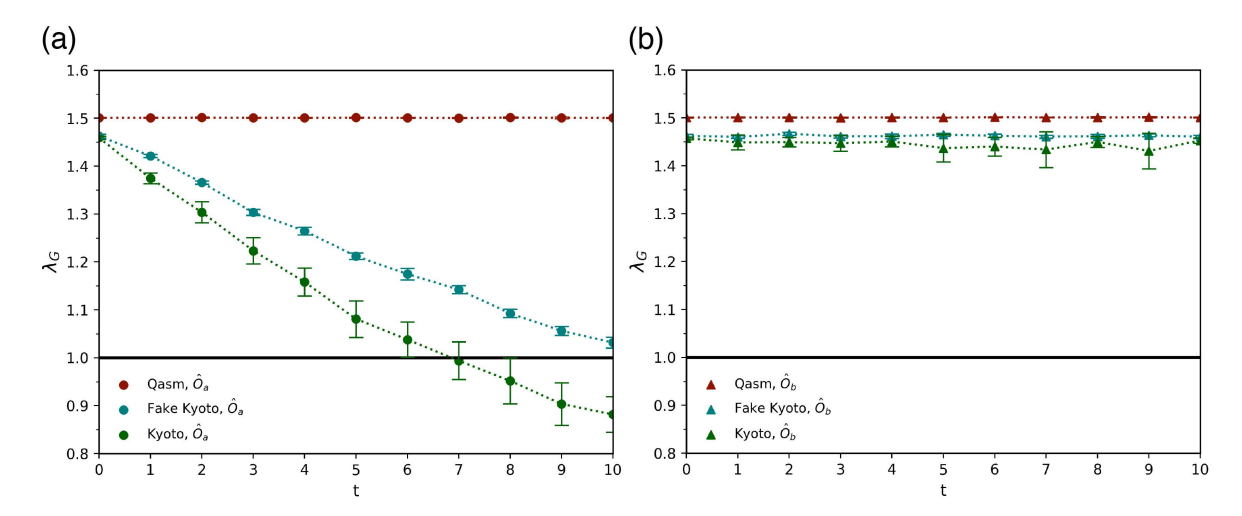


Figure 2: Decay trajectory of  $\lambda_G$  for  $\hat{O}_a$  (a) and  $\hat{O}_b$  (b), both with  $\omega=0.2$ . Trajectories from the ibm\_kyoto device are labelled "Kyoto", trajectories from the corresponding noise model are labelled "FakeKyoto", and trajectories from IBM's noise-free QASM simulator are labelled "QASM". The black line at  $\lambda_G=1.0$  indicates the noninteracting limit. Confidence intervals are calculated via the method described in the Supporting Information.

Comparing the modified particle-hole RDM  ${}^2\tilde{G}$  at t=0 and at t=10 in Figure 3, we observe the breakdown of the off-diagonal long-range order that leads to the formation of a condensate. While there are still some off-diagonal contributions from the terms corresponding to the population of a superposition between the  $|0\rangle$  and  $|1\rangle$  states for each qubit, the off-diagonal elements corresponding to entanglement between qubits all approach zero at t=10. This indicates that the transition previously observed in the orbital occupation numbers is a transition towards an incoherent ensemble state, rather than a different strongly correlated state.

For the noisy simulator,  $\lambda_G$  begins at a value of approximately 1.46, and after 10 time evolution steps decays to a value of approximately 1.03. The state fidelity at t = 0 is 0.955, showing that the prepared state is very similar to the ideal GHZ state, as in the case of the real device. As  $\lambda_G$  has not yet fallen below the threshold value of 1, the time evolution from the noisy simulator results in some condensate character remaining at t = 10. The decay of  $\lambda_G$  for the real device is notably steeper, suggesting that the noise model as constructed may

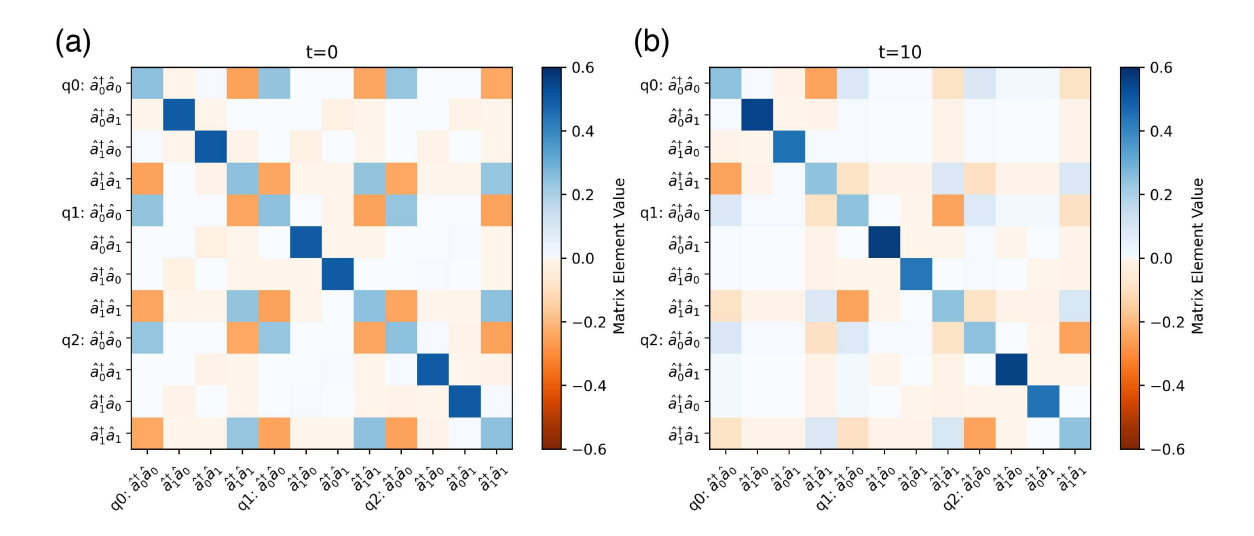


Figure 3: Heatmap representation of the modified particle-hole RDM  ${}^2\tilde{G}$ , after zero (a) and ten (b) timesteps from the propagation of  $\hat{O}_a$  on the real quantum device. Elements of  ${}^2\tilde{G}$  are given by eqs 4 and 5. For details of the tomography of the particle-hole RDM, see Ref. <sup>26</sup>

be unable to capture the full extent of device noise. The Qiskit noise model is constructed to include single- and two-qubit gate errors consisting of a depolarizing error followed by a relaxation error, as well as single qubit readout errors.<sup>57</sup> These parameters are derived from qubit and gate information ( $T_1$  and  $T_2$  times, frequency, readout error, gate error, and gate time) obtained via system snapshots. More complex errors such as those resulting from electromagnetic interference and undesired interactions or entanglement between qubits are not included. One side effect of this is that decoherence and dephasing on idle qubits is neglected, as those errors are mostly due to electromagnetic interference and cross-talk.<sup>58</sup> The inability of the noise model to account for the decoherence and dephasing of idle qubits, as well as other more complex interactions between system and bath, may account for the shallower decay of  $\lambda_G$  from FakeKyoto as compared to the real Kyoto device.

While  $\hat{O}_a$  results in a smooth decay of  $\lambda_G$  from 1.46 to 0.88,  $\lambda_G$  for  $\hat{O}_b$  does not decay but instead remains consistently in the realm of the initial value, 1.46. The plotted trajectory displays a slight oscillation, the result of significant oscillations present in some trials. The trajectory means and confidence intervals as plotted in Fig. 2 demonstrate that  $\hat{O}_a$  results in a reliable decay pattern of  $\lambda_G$ , while  $\hat{O}_b$  results in eigenvalues that do not decay significantly

from the initial value. The fact that  $\hat{O}_a$  results in swift decay of  $\lambda_G$  while  $\hat{O}_b$  does not decay suggests that the noise incurred by two-qubit CNOT operations cause a significant degradation of the system-wide entanglement, while the noise incurred by single-qubit  $R_Z$  rotations leaves the strongly correlated state essentially intact. The GHZ state preparations subject to  $\hat{O}_b$ , however, seem to be sensitive to some transient noise source that causes oscillations in the  $\lambda_G$  trajectory during some trials. The oscillations indicate the emergence of non-Markovian dynamics, wherein complex system-bath interactions cause a system to develop a "memory" such that the future state of the system depends on past states. Non-Markovianity is not visible in any trials for the  $\hat{O}_a$  case. Previous work has identified non-Markovian dynamics resulting from noise on quantum devices.<sup>28</sup>

A possible explanation for presence of non-Markovian character from the time evolution of  $\hat{O}_b$  but not from  $\hat{O}_a$  is that the six CNOT operations required for every application of  $\hat{O}_a$  cause swift relaxation and thus purely dissipative Markovian dynamics. The absence of such dominating two-qubit gate errors at every timestep in the case of  $\hat{O}_b$  means a much slower relaxation where more subtle non-Markovian effects manifest. The fact that non-Markovian characteristics are present in only some of the trials suggests that, upon variation of the noise environment of the device (and thus the system-bath interactions), the relative Markovianity of the dynamics may also be subject to variation. Plots of all trials for the  $\hat{O}_a$  and  $\hat{O}_b$  trajectories are available in the Supporting Information.

Non-Markovian character is not present in the  $\lambda_G$  trajectory from time evolution of  $\hat{O}_b$  on the noisy simulator, which is smooth and does not decay (seen in the turquoise data points in Figure 2). The failure of the noisy simulator to replicate the oscillatory behavior of  $\lambda_G$  for  $\hat{O}_b$  is likely because the noise model of FakeKyoto does not account for any non-Markovian noise. The presence of complex dynamical errors on quantum devices that are not captured by popular Markovian models is well documented, and the characterization of non-Markovian noise on quantum devices is an active field of study. <sup>59–63</sup> The construction of noise models that capture Markovian and non-Markovian noise will allow further investigation of

the impact of non-Markovian noise on the lifetime of strongly correlated states on quantum devices, and future work will explore this issue in more depth.

As expected, evolving the three-qubit GHZ state in time according to  $\hat{O}_a$  and  $\hat{O}_b$  with the noiseless QASM simulator<sup>56</sup> results in a  $\lambda_G$  that remains at the expected maximum value for 3 qubits, 1.5, for every step of the trajectory. These results confirm that all time dependence of the system results from device noise, and device noise alone is responsible for the decay of  $\lambda_G$  and thus the destruction of long-range order and system-wide entanglement.

The methodology used in the above three-qubit investigations is generalizable to any number of qubits, so it is of interest to see how the noise-triggered time dependence of the GHZ state is influenced by the number of qubits in the system. GHZ states are prepared with 4,5,6, and 10 qubits, then evolved in time via repeated unitary operations as described above. In each case  $\hat{O}_a$  is modified to include two-qubit tensor product terms for the additional qubits. These modified  $\hat{O}_a$ s, as well as schematics demonstrating their quantum state preparations, are available in the Supporting Information.  $\hat{O}_b$  is also modified by including an additional  $\sigma_z$  operation for each additional qubit.

The resulting trajectories of  $\lambda_G$  for each case are plotted in Figure 4, for an arbitrary  $\omega$  of 0.2. Due to limited computational time available, the noisy simulator is used for these investigations. The noisy simulator was previously shown to be suitable for replicating the general decay curve of  $\lambda_G$  for  $\hat{O}_a$ , and so the patterns resulting from these simulations are expected to hold for the real quantum device. While the noisy simulator is unable to replicate the oscillatory behavior seen in some trials of  $\hat{O}_b$ , it is still able to capture the fact that  $\lambda_G$  for  $\hat{O}_b$  does not decay but instead remains in the realm of the initial value. As such, we believe the noisy simulator provides a reasonable estimation of the  $\lambda_G$  trajectory for  $\hat{O}_b$  with increasing number of qubits, neglecting any non-Markovian effects.

By applying a nonlinear least-squares fit (to the exponential function  $y = ae^{bx}$ ), we see that  $\lambda_G$  trajectories from  $\hat{O}_a$  with increasing the number of qubits demonstrate steeper decay curves for increasing numbers of qubits. The decay rates from nonlinear least-squares

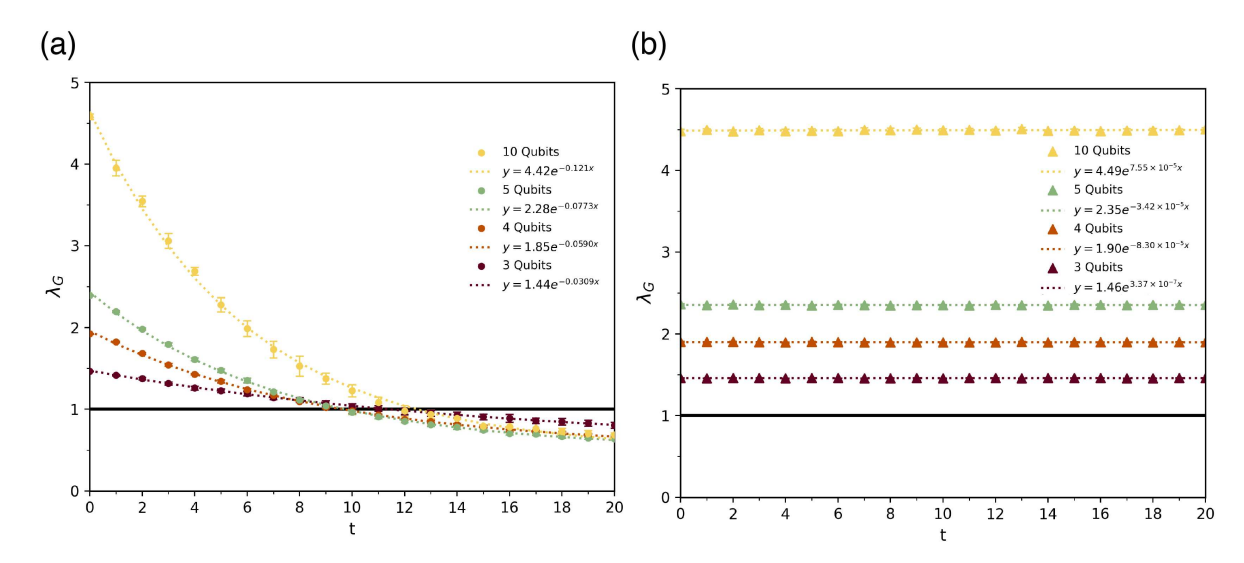


Figure 4: Decay trajectory of  $\lambda_G$  for  $\hat{O}_a$  (a) and  $\hat{O}_b$  (b) with 3,4,5, and 10 qubits ( $\omega = 0.2$ ). All trajectories from noisy simulations. Best-fit curves obtained via nonlinear least-squares fit. Confidence intervals are calculated via the method described in the Supporting Information.

fitting are -0.0309, -0.0590, -0.0773, and -0.121 for the 3-qubit, 4-qubit, 5-qubit, and 10qubit trajectories, respectively. All parameters obtained from the nonlinear least-squares fit, as well as standard deviation data for each parameter, are available in the Supporting Information. At t=0,  $\lambda_G$  begins at a greater value for increasing numbers of qubits (as the value of  $\lambda_G$  approaches the ideal value of  $\frac{N}{2}$  in each case, with N equal to the number of qubits). However, the increasing decay rate for larger numbers of qubits results in all eigenvalue trajectories falling below the threshold value of 1 by t=20. The steeper decay curves observed for larger numbers of qubits are likely due to the cumulative errors from the greater number of two-qubit gates required for propagating systems with increasing numbers of qubits. The resultant trajectories from  $O_b$  with increasing numbers of qubits demonstrate that, as in the 3-qubit case, the eigenvalue does not decay but remains very close to the initial value. Nonlinear least-squares fits demonstrate decay rates very close to zero for any number of qubits. While these results do not include any non-Markovian effects that may be present in the real device, they do support the idea that the minimal noise brought on by  $R_Z$  rotations is not sufficient to impact system-wide entanglement, even for states involving larger numbers of qubits.

## **Discussion and Conclusions**

Here we probe the lifetime of system-wide entanglement and long-range order in a strongly correlated state prepared on a NISQ-era quantum device. We find that noise on the device generates an effective bath which couples to the strongly correlated state, causing non-trivial time dependence observed in the breakdown of off-diagonal long-range order. The extraneous time evolution experienced by a stationary state indicates the presence of undesirable "fictitious forces" resulting from the complex combined effects of various error types including thermal decoherence and dephasing, depolarization, measurement errors, electromagnetic interference, inter-qubit cross-talk, and time-correlated system-bath interactions, which results in a transition from the desired state to an incoherent ensemble state. Understanding that quantum device noise causes a stationary state to develop non-trivial time dependence through the disruption of strong correlation provides insight into the challenges faced in simulating strongly correlated systems on quantum devices. Furthermore, our results high-light the severe restrictions faced in designing algorithms for reliable simulation of quantum chemical systems on current quantum computers.

We observe off-diagonal long-range order being completely extinguished in only ten timesteps for a three-qubit GHZ state, corresponding to 30 CNOT gate applications. This underscores the restrictions in algorithm design faced if one hopes to accurately model a strongly-correlated quantum system on a near-term quantum computer, as each two-qubit gate progressively destroys the correlation in the system. Single-qubit gate errors, however, do not appear to extinguish the system-wide entanglement in the way that two-qubit gate errors do. The impact of system size on the decay of  $\lambda_G$  presents an additional obstacle for simulating quantum chemical systems—achieving system-wide entanglement and off-diagonal long-range order for increasing numbers of qubits will require increasing numbers of two-qubit gates, which in turn causes swifter breakup of system-wide entanglement and off-diagonal long-range order. Together, the compounding destruction of correlation caused by qubit number and circuit size emphasizes the necessity of developing novel strategies

for error mitigation that can preserve many-body correlation and minimize undesired time evolution brought on by noise.

The investigations presented here all involve the case where the strongly correlated system is a stationary state, and thus all time dependence is the result of noise. However, the knowledge that device noise causes extraneous time evolution in even in stationary simulations suggests that such "fictitious forces" brought on by noise will impact the dynamics of a time-dependent calculation. This motivates future investigations into the effect of device noise on a strongly correlated system undergoing a driven process. Such investigations could provide important insight into the particular challenges faced in modeling time-dependent processes on quantum computers.

# Acknowledgement

D.A.M. gratefully acknowledges support from the Department of Energy, Office of Basic Energy Sciences, Grant DE-SC0019215, the ACS Petroleum Research Fund Grant No. PRF No. 61644-ND6, the U. S. National Science Foundation Grant Nos. CHE-2155082 and DMR-2037783, and the U.S. National Science Foundation (NSF) QuBBE Quantum Leap Challenge Institute (NSF Grant No. OMA-2121044). We acknowledge the use of IBM Quantum services for this work. The views expressed are those of the authors, and do not reflect the official policy or position of IBM or the IBM Quantum team.

# Supporting Information Available

Detailed quantum state preparation, heatmap plots of  ${}^2\tilde{G}$  for t=0 and t=10 from noisy simulator, plots of all ten eigenvalue trajectory trials from  $\hat{O}_a$  and  $\hat{O}_b$ , plots of  $\lambda_G$  for increasing numbers of qubits including trajectories from the noiseless QASM simulator, statistical methods, device calibration data for ibm\_kyoto, discussion of the varieties of quantum device error, and details of the nonlinear least-squares fitting procedure.

## References

- (1) Lee, P. A. From high temperature superconductivity to quantum spin liquid: progress in strong correlation physics. *Reports on Progress in Physics* **2008**, *71*, 012501.
- (2) Lee, P. A.; Nagaosa, N.; Wen, X.-G. Doping a Mott insulator: Physics of high-temperature superconductivity. *Reviews of Modern Physics* **2006**, *78*, 17–85.
- (3) Garg, A.; Randeria, M.; Trivedi, N. Strong correlations make high-temperature super-conductors robust against disorder. *Nature Physics* **2008**, *4*, 762–765.
- (4) Hohenadler, M.; Assaad, F. F. Correlation effects in two-dimensional topological insulators. *Journal of Physics: Condensed Matter* **2013**, *25*, 143201.
- (5) Toklikishvili, Z.; Chotorlishvili, L.; Stagraczyński, S.; Dugaev, V. K.; Ernst, A.; Barnaś, J.; Berakdar, J. Effects of spin-dependent electronic correlations on surface states in topological insulators. *Physical Review B* 2019, 100, 235419.
- (6) Feynman, R. P. Simulating physics with computers. International Journal of Theoretical Physics 1982, 21, 467–488.
- (7) Elfving, V. E.; Broer, B. W.; Webber, M.; Gavartin, J.; Halls, M. D.; Lorton, K. P.; Bochevarov, A. How will quantum computers provide an industrially relevant computational advantage in quantum chemistry? **2020**, Publisher: arXiv Version Number: 1.
- (8) Kassal, I.; Whitfield, J. D.; Perdomo-Ortiz, A.; Yung, M.-H.; Aspuru-Guzik, A. Simulating Chemistry Using Quantum Computers. *Annual Review of Physical Chemistry* **2011**, *62*, 185–207.
- (9) Aspuru-Guzik, A.; Dutoi, A. D.; Love, P. J.; Head-Gordon, M. Simulated Quantum Computation of Molecular Energies. *Science* **2005**, *309*, 1704–1707.

- (10) McArdle, S.; Endo, S.; Aspuru-Guzik, A.; Benjamin, S. C.; Yuan, X. Quantum computational chemistry. *Reviews of Modern Physics* **2020**, *92*, 015003.
- (11) Head-Marsden, K.; Flick, J.; Ciccarino, C. J.; Narang, P. Quantum Information and Algorithms for Correlated Quantum Matter. *Chemical Reviews* **2021**, *121*, 3061–3120.
- (12) Verstraete, F.; Cirac, J. I.; Latorre, J. I. Quantum circuits for strongly correlated quantum systems. *Physical Review A* **2009**, *79*, 032316.
- (13) Paesani, S.; Gentile, A.; Santagati, R.; Wang, J.; Wiebe, N.; Tew, D.; O'Brien, J.; Thompson, M. Experimental Bayesian Quantum Phase Estimation on a Silicon Photonic Chip. *Physical Review Letters* **2017**, *118*, 100503.
- (14) Du, J.; Xu, N.; Peng, X.; Wang, P.; Wu, S.; Lu, D. NMR Implementation of a Molecular Hydrogen Quantum Simulation with Adiabatic State Preparation. *Physical Review Letters* **2010**, *104*, 030502.
- (15) Peruzzo, A.; McClean, J.; Shadbolt, P.; Yung, M.-H.; Zhou, X.-Q.; Love, P. J.; Aspuru-Guzik, A.; O'Brien, J. L. A variational eigenvalue solver on a photonic quantum processor. *Nature Communications* **2014**, *5*, 4213.
- (16) Wecker, D.; Hastings, M. B.; Troyer, M. Progress towards practical quantum variational algorithms. *Physical Review A* **2015**, *92*, 042303.
- (17) McClean, J. R.; Romero, J.; Babbush, R.; Aspuru-Guzik, A. The theory of variational hybrid quantum-classical algorithms. *New Journal of Physics* **2016**, *18*, 023023.
- (18) Kandala, A.; Mezzacapo, A.; Temme, K.; Takita, M.; Brink, M.; Chow, J. M.; Gambetta, J. M. Hardware-efficient variational quantum eigensolver for small molecules and quantum magnets. *Nature* **2017**, *549*, 242–246.
- (19) Wang, D.; Higgott, O.; Brierley, S. Accelerated Variational Quantum Eigensolver. *Physical Review Letters* **2019**, *122*, 140504.

- (20) Smart, S. E.; Mazziotti, D. A. Quantum Solver of Contracted Eigenvalue Equations for Scalable Molecular Simulations on Quantum Computing Devices. *Physical Review Letters* **2021**, *126*, 070504.
- (21) Smart, S. E.; Mazziotti, D. A. Many-fermion simulation from the contracted quantum eigensolver without fermionic encoding of the wave function. *Physical Review A* **2022**, 105, 062424.
- (22) Smart, S. E.; Mazziotti, D. A. Verifiably exact solution of the electronic Schrödinger equation on quantum devices. *Physical Review A* **2024**, *109*, 022802.
- (23) Breuer, H.-P.; Petruccione, F. *The theory of open quantum systems*, repr ed.; Clarendon Press: Oxford, 2010.
- (24) Schlosshauer, M. Quantum decoherence. Physics Reports 2019, 831, 1–57.
- (25) Clerk, A. A.; Devoret, M. H.; Girvin, S. M.; Marquardt, F.; Schoelkopf, R. J. Introduction to quantum noise, measurement, and amplification. *Reviews of Modern Physics* **2010**, *82*, 1155–1208.
- (26) Sager, L. M.; Smart, S. E.; Mazziotti, D. A. Preparation of an exciton condensate of photons on a 53-qubit quantum computer. *Physical Review Research* **2020**, 2, 043205.
- (27) Sager-Smith, L. M.; Smart, S. E.; Mazziotti, D. A. Qubit Condensation for Assessing Efficacy of Molecular Simulation on Quantum Computers. *The Journal of Physical Chemistry A* **2023**, *127*, 6032–6039.
- (28) Smart, S. E.; Hu, Z.; Kais, S.; Mazziotti, D. A. Relaxation of stationary states on a quantum computer yields a unique spectroscopic fingerprint of the computer's noise. *Communications Physics* **2022**, *5*, 28.

- (29) Sun, J.; Yuan, X.; Tsunoda, T.; Vedral, V.; Benjamin, S. C.; Endo, S. Mitigating Realistic Noise in Practical Noisy Intermediate-Scale Quantum Devices. *Physical Review Applied* **2021**, *15*, 034026.
- (30) Kandala, A.; Temme, K.; Córcoles, A. D.; Mezzacapo, A.; Chow, J. M.; Gambetta, J. M. Error mitigation extends the computational reach of a noisy quantum processor. *Nature* **2019**, *567*, 491–495.
- (31) McArdle, S.; Yuan, X.; Benjamin, S. Error-Mitigated Digital Quantum Simulation.

  Physical Review Letters 2019, 122, 180501.
- (32) Endo, S.; Cai, Z.; Benjamin, S. C.; Yuan, X. Hybrid Quantum-Classical Algorithms and Quantum Error Mitigation. *Journal of the Physical Society of Japan* **2021**, *90*, 032001.
- (33) Smart, S. E.; Boyn, J.-N.; Mazziotti, D. A. Resolving correlated states of benzyne with an error-mitigated contracted quantum eigensolver. *Physical Review A* **2022**, *105*, 022405.
- (34) Smart, S. E.; Mazziotti, D. A. Quantum-classical hybrid algorithm using an error-mitigating N -representability condition to compute the Mott metal-insulator transition. *Physical Review A* **2019**, *100*, 022517.
- (35) Preskill, J. Quantum Computing in the NISQ era and beyond. Quantum 2018, 2, 79.
- (36) Wang, R.; Zhao, P.; Jin, Y.; Yu, H. Control and mitigation of microwave crosstalk effect with superconducting qubits. *Applied Physics Letters* **2022**, *121*, 152602.
- (37) Li, Y.; Benjamin, S. C. Efficient Variational Quantum Simulator Incorporating Active Error Minimization. *Physical Review X* **2017**, *7*, 021050.
- (38) Temme, K.; Bravyi, S.; Gambetta, J. M. Error Mitigation for Short-Depth Quantum Circuits. *Physical Review Letters* **2017**, *119*, 180509.

- (39) Strikis, A.; Qin, D.; Chen, Y.; Benjamin, S. C.; Li, Y. Learning-Based Quantum Error Mitigation. *PRX Quantum* **2021**, *2*, 040330.
- (40) Ma, R.; Saxberg, B.; Owens, C.; Leung, N.; Lu, Y.; Simon, J.; Schuster, D. I. A dissipatively stabilized Mott insulator of photons. *Nature* **2019**, *566*, 51–57.
- (41) Sager, L. M.; Mazziotti, D. A. Cooper-pair condensates with nonclassical long-range order on quantum devices. *Physical Review Research* **2022**, *4*, 013003.
- (42) Sager, L. M.; Mazziotti, D. A. Entangled phase of simultaneous fermion and exciton condensations realized. *Physical Review B* **2022**, *105*, L121105.
- (43) Safaei, S.; Mazziotti, D. A. Quantum signature of exciton condensation. *Physical Review B* **2018**, *98*, 045122.
- (44) Garrod, C.; Rosina, M. Particle-Hole Matrix: Its Connection with the Symmetries and Collective Features of the Ground State. *Journal of Mathematical Physics* 1969, 10, 1855–1861.
- (45) Kohn, W.; Sherrington, D. Two Kinds of Bosons and Bose Condensates. *Reviews of Modern Physics* **1970**, *42*, 1–11.
- (46) Borland, R. E.; Dennis, K. The conditions on the one-matrix for three-body fermion wavefunctions with one-rank equal to six. *Journal of Physics B: Atomic and Molecular Physics* 1972, 5, 7–15.
- (47) The physical interpretation of the quantum dynamics. Proceedings of the Royal Society of London. Series A, Containing Papers of a Mathematical and Physical Character 1927, 113, 621–641.
- (48) Heisenberg, W. Mehrkörperproblem und Resonanz in der Quantenmechanik. Zeitschrift für Physik 1926, 38, 411–426.

- (49) Smart, S. E.; Schuster, D. I.; Mazziotti, D. A. Experimental data from a quantum computer verifies the generalized Pauli exclusion principle. *Communications Physics* **2019**, 2, 11.
- (50) Schilling, C.; Gross, D.; Christandl, M. Pinning of Fermionic Occupation Numbers.

  Physical Review Letters 2013, 110, 040404.
- (51) Benavides-Riveros, C. L.; Gracia-Bondía, J. M.; Springborg, M. Quasipinning and entanglement in the lithium isoelectronic series. *Physical Review A* **2013**, *88*, 022508.
- (52) Chakraborty, R.; Mazziotti, D. A. Generalized Pauli conditions on the spectra of oneelectron reduced density matrices of atoms and molecules. *Physical Review A* **2014**, *89*, 042505.
- (53) Mazziotti, D. A. Pure- N -representability conditions of two-fermion reduced density matrices. *Physical Review A* **2016**, *94*, 032516.
- (54) Mazziotti, D. A. Structure of Fermionic Density Matrices: Complete N Representability Conditions. *Physical Review Letters* **2012**, *108*, 263002.
- (55) Contributers, Q. Qiskit: An Open-source Framework for Quantum Computing. 2023,
- (56) Qiskit QasmSimulator, Qiskit Aer 0.13.1 Documentation. 2023; https://qiskit.org/ecosystem/aer/stubs/qiskit\_aer.QasmSimulator.html.
- (57) Qiskit Noise Models, Qiskit Aer 0.13.2 Documentation. 2023; https://qiskit.github.io/qiskit-aer/stubs/qiskit\_aer.noise.NoiseModel.html#qiskit\_aer.noise.NoiseModel.from\_backend.
- (58) Georgopoulos, K.; Emary, C.; Zuliani, P. Modeling and simulating the noisy behavior of near-term quantum computers. *Physical Review A* **2021**, *104*, 062432.
- (59) Gulácsi, B.; Burkard, G. Signatures of non-Markovianity of a superconducting qubit. *Physical Review B* **2023**, *107*, 174511.

- (60) White, G. A. L.; Hill, C. D.; Pollock, F. A.; Hollenberg, L. C. L.; Modi, K. Demonstration of non-Markovian process characterisation and control on a quantum processor.

  Nature Communications 2020, 11, 6301.
- (61) White, G.; Pollock, F.; Hollenberg, L.; Modi, K.; Hill, C. Non-Markovian Quantum Process Tomography. *PRX Quantum* **2022**, *3*, 020344.
- (62) Chen, Y.-Q.; Ma, K.-L.; Zheng, Y.-C.; Allcock, J.; Zhang, S.; Hsieh, C.-Y. Non-Markovian Noise Characterization with the Transfer Tensor Method. *Physical Review Applied* **2020**, *13*, 034045.
- (63) Pollock, F. A.; Rodríguez-Rosario, C.; Frauenheim, T.; Paternostro, M.; Modi, K. Non-Markovian quantum processes: Complete framework and efficient characterization. Physical Review A 2018, 97, 012127.

# TOC Graphic

